Available online at www.sciencedirect.com
ScienceDirect
Acta Materialia xxx (2008) xxx–xxx
Acta MATERIALIA
www.elsevier.com/locate/actamat

High-strain-rate response of ultra-fine-grained copper

A. Mishra [a], M. Martin [c], N.N. Thadhani [c], B.K. Kad [b], E.A. Kenik [d], M.A. Meyers [a,*]

[a] *Materials Science and Engineering Program, Departments of Mechanical and Aerospace Engineering and Nanoengineering, University of California, San Diego, La Jolla, CA 92093, USA*
[b] *Department of Structural Engineering, University of California, San Diego, La Jolla, CA 92093, USA*
[c] *School of Materials Science and Engineering, Georgia Institute of Technology, Atlanta, GA 30332, USA*
[d] *Oak Ridge National Laboratory, Oak Ridge, TN 37830, USA*

Received 31 October 2007; received in revised form 6 February 2008; accepted 8 February 2008

Abstract

The high-strain-rate response of ultra-fine-grained (UFG) copper processed by equal channel angular pressing (ECAP) was characterized by three different dynamic testing methods: reverse Taylor impact, cylindrical compression specimens, and hat-shaped specimens in Hopkinson bar experiments. Upon recovery after impact, the specimens were found to undergo dynamic recrystallization at a calculated temperature of 360 K, indicating that the UFG copper is thermally unstable. Reverse Taylor tests were conducted on as-received oxygen-free high-conductivity copper rod and ECAP specimens with 2 and 8 sequential deformation passes. The dynamic deformation of the samples was modeled using AUTODYN-2D, and a modified Johnson–Cook constitutive equation was found to closely capture the dynamic response. Both the dynamic experiments and analysis from the reverse Taylor tests indicate enhanced strain-rate sensitivity in comparison with conventional polycrystalline copper, in agreement with predictions of reduced activation volume. The shear band thickness, as obtained in forced localization tests, showed a marked decrease, in comparison to conventional polycrystalline copper; this effect is interpreted as due to an accelerated thermal softening and inherent instability exhibited by the UFG structure.

Keywords: Severe plastic deformation (SPD); Equal channel angular pressing (ECAP); Recrystallization; Finite element analysis

1. Introduction

Nanocrystalline and ultra-fine-grained (UFG) metals have unique mechanical properties (strength, hardness, fatigue resistance) that have been the subject of widespread research [1–5]. Although the quasistatic mechanical response of these materials has been studied in great detail, the corresponding response at high-strain-rates is still less well known. Gray et al. [6] reported a higher strain-rate sensitivity of UFG copper in comparison with fully annealed polycrystalline copper. This effect has been explained by the inverse relationship between the strain-rate sensitivity, defined as $\partial \ln \sigma / \partial \ln \dot{\varepsilon}$, and activation volume for plastic deformation; the latter decreases significantly in face-centered cubic (fcc) metals at small grain sizes, due to a presumed change in rate-controlling mechanism from forest dislocation intersection to emission of dislocations from grain-boundary sources. Thus, the strain-rate sensitivity is increased (e.g. [4,6–10]).

A topic of recent significance and concern is the thermal stability of UFG and nano-structured materials. Thermal stability is an important issue that needs to be addressed for the suitability of these materials in structural applications. The severe plastic deformation techniques and, in particular, equal channel angular pressing (ECAP), are known to produce grain sizes in the range of 200–500 nm with high density of high-angle grain boundaries and saturated dislocation density (e.g., [11–19]). Inherently, in single-phase pure metals, such a microstructure is thermally unstable and the propensity for heat-induced recrystallization is high. Indeed, Mishra et al. [20] showed that grain

* Corresponding author. Tel.: +1 619 534 5698x07.
E-mail address: mameyers@ucsd.edu (M.A. Meyers).

1359-6454/$34.00 © 2008 Acta Materialia Inc. Published by Elsevier Ltd. All rights reserved.
doi:10.1016/j.actamat.2008.02.023

boundaries can exhibit considerable mobility at temperatures as low as 360 K in UFG copper.

This paper addresses the issues of strain-rate sensitivity and thermal stability in pure copper processed by ECAP. A series of high-strain-rate deformation tests were carried out via three different techniques (cylindrical and hat-shaped Hopkinson bar and reverse Taylor tests).

2. Experimental procedure

Commercially obtained cold-rolled oxygen-free high-conductivity (OFHC) Cu rods were processed using a horizontal split ECAP die with an interior channel angle of 102° and an external arc of curvature of 20°. A series of samples with 0, 2 and 8 passes were processed using route B_C. In route B_C the specimen is rotated 90° about its longitudinal axis after each pass. The experimental set-up for ECAP was explained earlier [20]. The Route B_C was found to yield most equiaxed grains. For the Hopkinson bar tests, two kinds of samples were machined: cylindrical specimens with dimensions of 4×4 mm and hat-shaped specimens with dimensions as indicated in Fig. 1a. The hat-shape design [21] has been used extensively to study adiabatic shear bands in BCC steel [22,23], tantalum [24,25]; fcc cop-

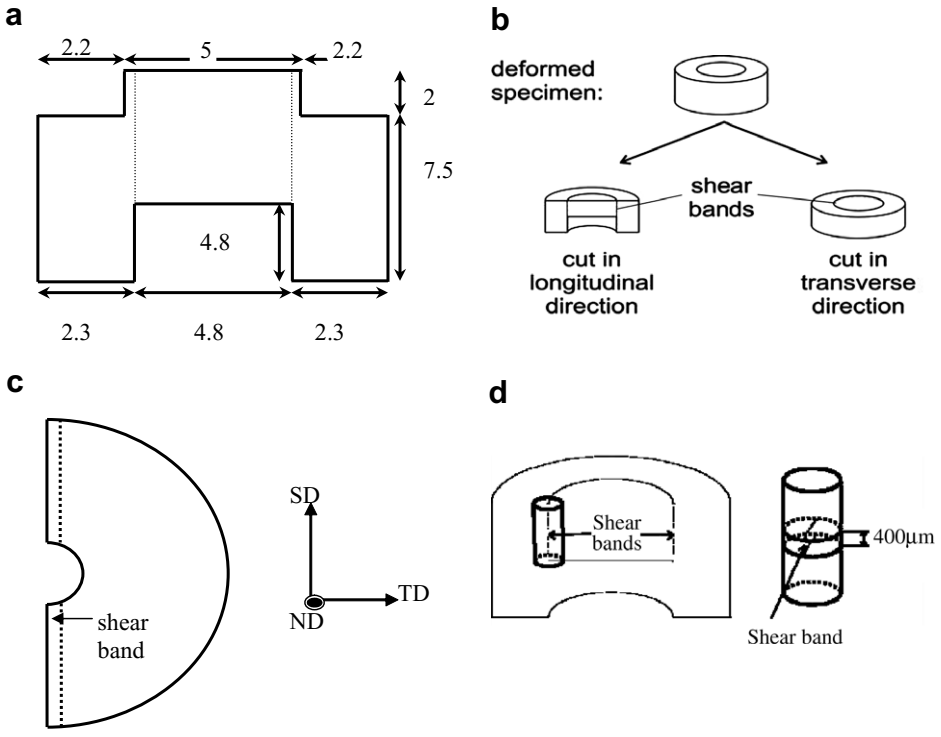

Fig. 1. (a) Geometry of the hat-shaped specimen (all dimensions are in mm); (b) longitudinal and transverse cuts; (c) three orientations of EBSD characterization; and (d) extraction of TEM specimens.

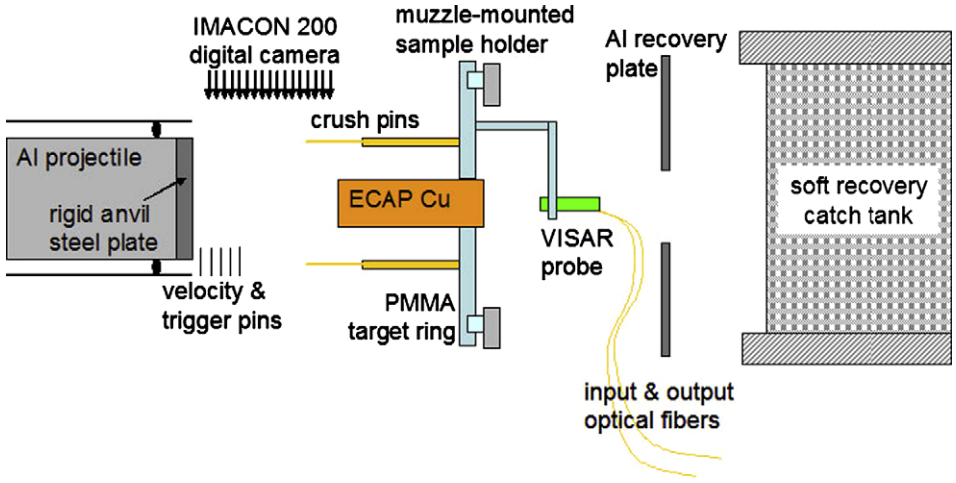

Fig. 2. Schematic of reverse Taylor anvil-on-rod impact test setup.

Please cite this article in press as: Mishra A et al., High-strain-rate response of ultra-fine-grained copper, Acta Mater (2008), doi:10.1016/j.actamat.2008.02.023

per [26,27], aluminum alloys [28], austenitic stainless steel [29,30]; hexagonal close-packed titanium [31], and zirconium [32]. The specimen shape, Fig. 1, is designed to concentrate deformation in a narrow zone facilitating the formation of a shear band. Compression tests on cylindrical samples were performed at strain rates of 5×10^{-3}, 0.1 and 10^2 s^{-1}.

For Taylor tests [33], cylindrical rod samples of 9.4 mm diameter and 40.13 mm length were machined. The rods were lapped on both ends with 45 μm diamond suspension to insure parallel and polished surfaces. A schematic of the reverse Taylor impact test setup is shown in Fig. 2. The projectile consists of a 2024-Al 80 mm diameter sabot with a maraging steel rigid anvil plate secured to the front surface. The rod-shaped samples were mounted to a target ring and aligned with a laser beam to ensure parallel impact. An IMACON-200 high-speed digital camera was used to capture images of the deformation of the rods

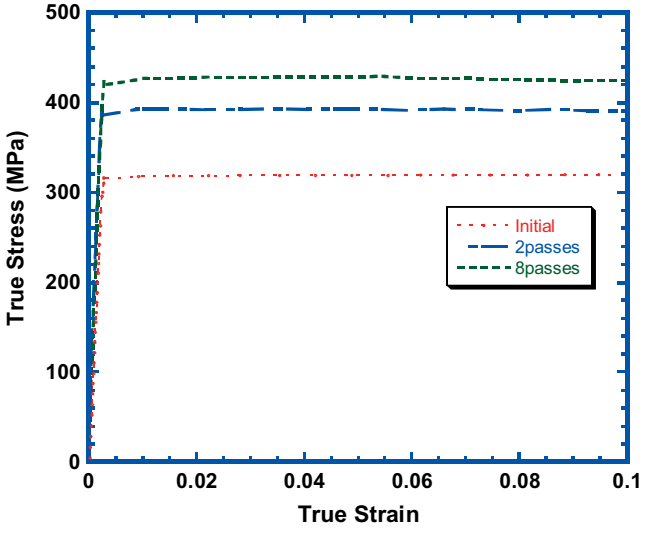

Fig. 3. Quasistatic true stress-true strain plots for Cu samples in as-received state and after 2 and 8 ECAP passes ($\dot{\varepsilon} = 0.1$ s^{-1}).

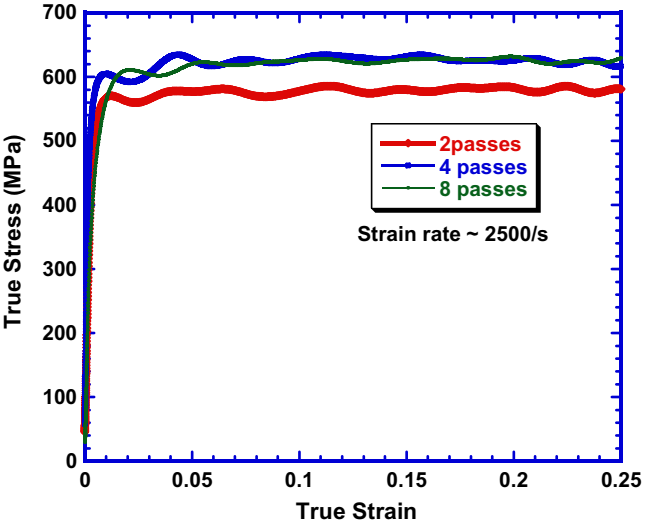

Fig. 4. Dynamic true stress-true strain plots for the initial, 2 and 8 pass ECAP samples ($\dot{\varepsilon} = 2500$ s^{-1}).

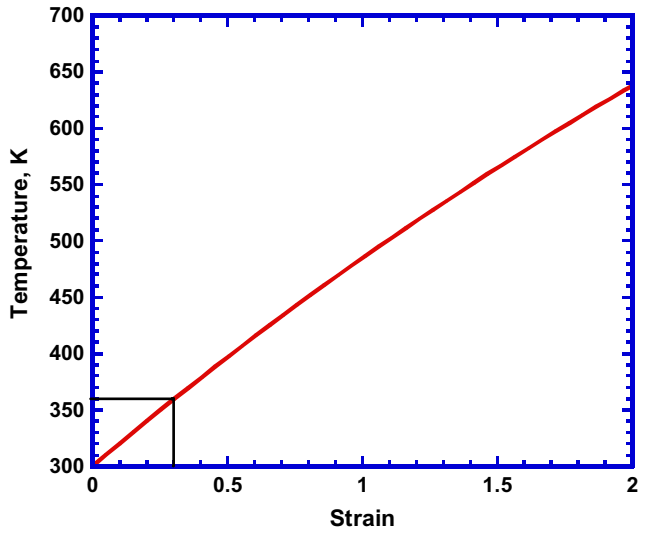

Fig. 5. Temperature as a function of strain for strain rate $\dot{\varepsilon} \approx 10^3$ s^{-1}, characteristic of cylindrical specimens in Hopkinson bar test (for a strain of 0.3 as in the case of cylindrical specimens, $T = 360$ K).

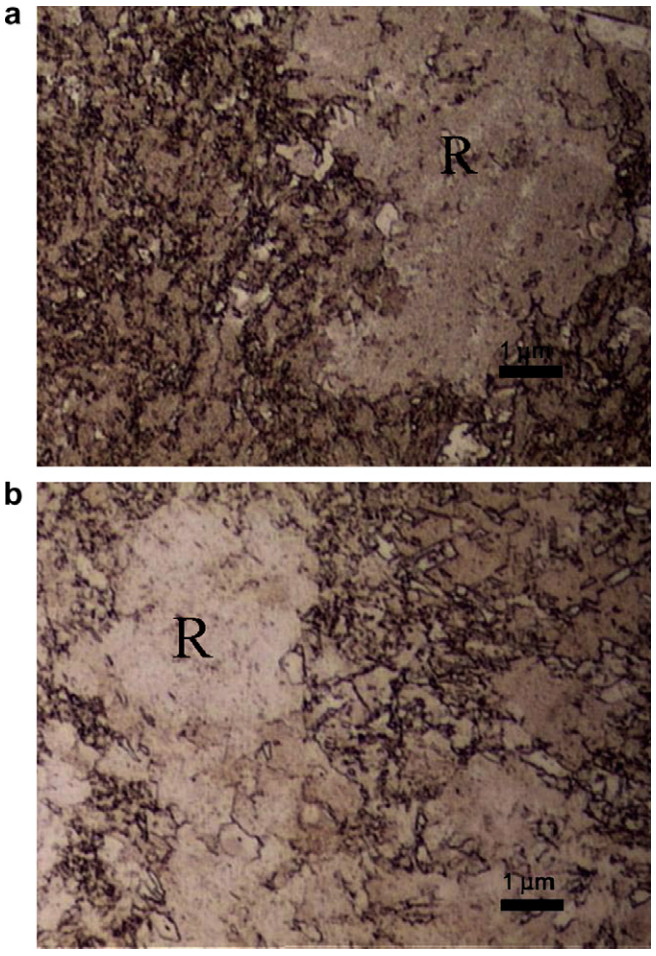

Fig. 6. Recrystallized microstructure upon compression testing (recrystallized regions denoted by "*R*").

Please cite this article in press as: Mishra A et al., High-strain-rate response of ultra-fine-grained copper, Acta Mater (2008), doi:10.1016/j.actamat.2008.02.023

during impact by the projectile. Velocity interferometry (VISAR) (placement shown in Fig. 2) was also used to capture the free surface velocity of the tested rod.

AUTODYN simulations of the anvil-on-rod impact experiments were performed to validate the constitutive response of the specimens as a function of strain ε using the Johnson–Cook [34] constitutive equation

$$\sigma = [A + B\varepsilon^n][1 + C\ln\dot{\varepsilon}^*][1 - T^{*m}], \quad (1)$$

where A, B, C, n, and m are experimentally determined parameters. The unknown strain-rate sensitivity, C, was obtained by fitting the simulated free surface velocity trace to that determined experimentally using VISAR, as described by Eakins and Thadhani [35] and Martin et al. [36]. The models were further validated by comparing the simulated transient deformation profiles with the images captured during deformation. Simulations were run in two dimensions as an axi-symmetric problem, and gauges were placed on the specimen's back surface to track the free surface velocity.

The microstructure of the hat-shaped tested sample was characterized using optical microscopy (OM), electron backscattering diffraction (EBSD), and transmission electron microscopy (TEM). Fig. 1b shows how specimens were machined out of the hat-shaped sample for microstructural examination. EBSD examination was performed in the undeformed regions and in areas close to the shear band using a Philips XL 30 scanning electron microscope operating at 15 kV and TSL indexing software. A 3 mm disk (cut as shown in Fig. 1d) was electropolished using 7% H_2SO_4 and placed in the SEM sample holder as shown in Fig. 1c, i.e. the normal, transverse, and shear (longitudinal) directions in the EBSD maps.

Specimens for TEM examination were obtained from the same 3 mm diameter cylinder. Disks for TEM foils were machined in such a way that the shear band was off-center as shown in Fig. 1d. Since electropolishing creates a hole in the center of the sample, this ensured that there existed a region around the shear band that could be examined under TEM. Disks with thickness of 300 μm were cut and polished down to 100 μm using 2400 and 4000 grid SiC papers. Final thinning to electron transparency was achieved by electropolishing in a solution containing 7 vol.% H_2SO_4 in methanol at –35 °C/25 V. Subsequently, as needed, the perforated disks were progressively ion-milled using a Gatan PIPS unit at ambient conditions until the perforation grew to the edge of the shear band.

Thin foils were prepared for TEM examination by using a twin-jet Struers Tenupol-3 polisher with an electro-polishing solution composed of 7 vol.% sulfuric acid in methanol at a temperature of –40 °C. TEM analysis was carried out on a Philips CM-30 (facility at ORNL, Tennessee) operating at 300 kV. Observations were made on both transverse and longitudinal directions in a series of samples with different number of ECAP passes.

3. Results and discussion

3.1. Cylindrical specimens

Fig. 3 shows the quasistatic true stress–true strain curves for initial, 2- and 8-pass ECAP Cu at a strain rate of 0.1 s^{-1}. ECAP samples having undergone significant deformation during processing as expected exhibited higher flow stresses. Each additional pass adds to the cumulative strain via dislocation generation and additional grain refinement. For example, the initial grain size of ~30 μm was reduced to ~200 nm after 8 ECAP passes. We note here that the initial cold-rolled Cu sample also exhibited an extensive deformation substructure consistent with the near zero work-hardening observed in the corresponding stress–strain curves. This was analyzed in greater detail by Mishra et al. [20].

Results from the dynamic compression tests carried out at a strain rate of 2500 s^{-1} are plotted in Fig. 4. There was a significant increase in strength at high-strain rate as compared to the quasistatic tests since UFG metals (like fcc copper) are known to have a higher strain-rate sensitivity than their coarse-grained counterpart. This topic is addressed in detail in Section 3.3.

The temperature rise in the Hopkinson bar test can be calculated from the constitutive response of copper which is also applicable to shear localization process. The temperature rise, ΔT_d (e.g. [8,25]) can be expressed as a function of strain:

$$\Delta T_d = \frac{\beta}{\rho C_p}\int_{\varepsilon_o}^{\varepsilon_1} \sigma \cdot d\varepsilon, \quad (2)$$

where ρ is the density, C_p the heat capacity, and β is the Taylor factor. Using Johnson–Cook equation [34] as the constitutive equation for the response and assuming that 90% of the work of deformation goes into heating, i.e., $\beta = 0.9$, the temperature change due to plastic deformation can be expressed as [37]:

$$\Delta T_d = 1 - \exp\left[\frac{-0.9\left(1 + C\log\frac{\dot{\varepsilon}}{\dot{\varepsilon}_0}\right)}{\rho C_p(T_m - T_r)} \times \left(\sigma_0\varepsilon + \frac{B\varepsilon^{n+1}}{n+1}\right)\right], \quad (3)$$

where in our case, $T_r = 300$ K, $T_m = 1356$ K, $B = 292$ MPa, $C_p = 394$ J (kg K)$^{-1}$, $\rho = 8.97 \times 10^3$ kg m^{-3}, $C = 0.025$, and $\sigma_0 = 400$ MPa. Since the work-hardening in the UFG specimens is negligible, $n = 0$.

Using Eq. (3), temperature is plotted as a function of strain (Fig. 5). For the cylindrical compression samples, at a strain $\varepsilon = 0.3$, the temperature in the sample was calculated to be 360 K (60 K above room temperature). The thermal stability of these samples was investigated using optical microscopy and is presented in Fig. 6. Large regions of recrystallized microstructure were observed adjacent to the UFG microstructure. Recrystallization studies on ECAP copper including texture have been reported in

Please cite this article in press as: Mishra A et al., High-strain-rate response of ultra-fine-grained copper, Acta Mater (2008), doi:10.1016/j.actamat.2008.02.023

several recent publications [38–42]. Estrin et al. [40] reported grain coarsening in ECAP copper resulting from natural aging at room temperature. Modolova et al. [38] calculated the driving force due to dislocation density in ECAP samples and found it to be higher than the driving force due to grain boundary energy. Mishra et al. [20] reported a dislocation density of 2×10^{15} m^{-2} and an average grain size of 200 nm in ECAP copper after 8 passes. From their reported values, the driving force due to boundary curvature turns out to be larger than the driving force for recrystallization due to dislocation density differences.

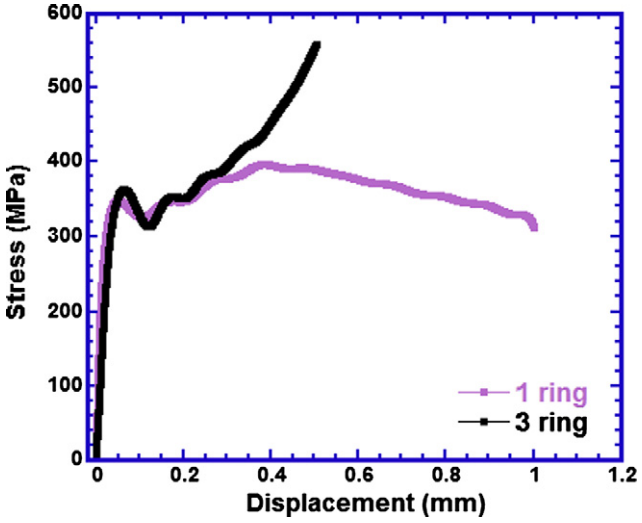

Fig. 7. Shear stress- shear strain plot for the hat shaped specimen.

Mishra et al. [20] reported a high density of high angle boundaries in samples with a large number of ECAP passes (the sequence follows as: large grain size and high density of high angle GBs in the initial sample → high density of low angle GBs after few ECAP passes → small grain size with high density of high angle GBs after large number of passes). This supports the argument that the activation energy of recrystallization is low in severely deformed samples, owing to the high density of high-angle grain boundaries that facilitates nucleation.

Murr and coworkers [43–46] have carried out extensive experiments on dynamic recrystallization induced by high-rate plastic deformation in both ballistic impact and friction stir-welding. The association of recrystallization with the dynamic deformation process is undeniable in the regime of severe plastic deformation (SPD). Thus, the term dynamic recrystallization refers to the complex interplay between the high-strain, high-strain-rate deformation and thermal recovery processes taking place concurrently or sequentially. We adopt here their broader definition of dynamic recrystallization (DRX).

3.2. Hat-shaped specimens

The shear stress–strain response of UFG hat-shaped sample tested by Hopkinson bar is shown in Fig. 7. The peak shear stress is 340 MPa, which translates to 680 MPa normal stresses. This is the range of strength for ECAP Cu as can be verified from Fig. 4. Once the hat is completely compressed, the load rises since the

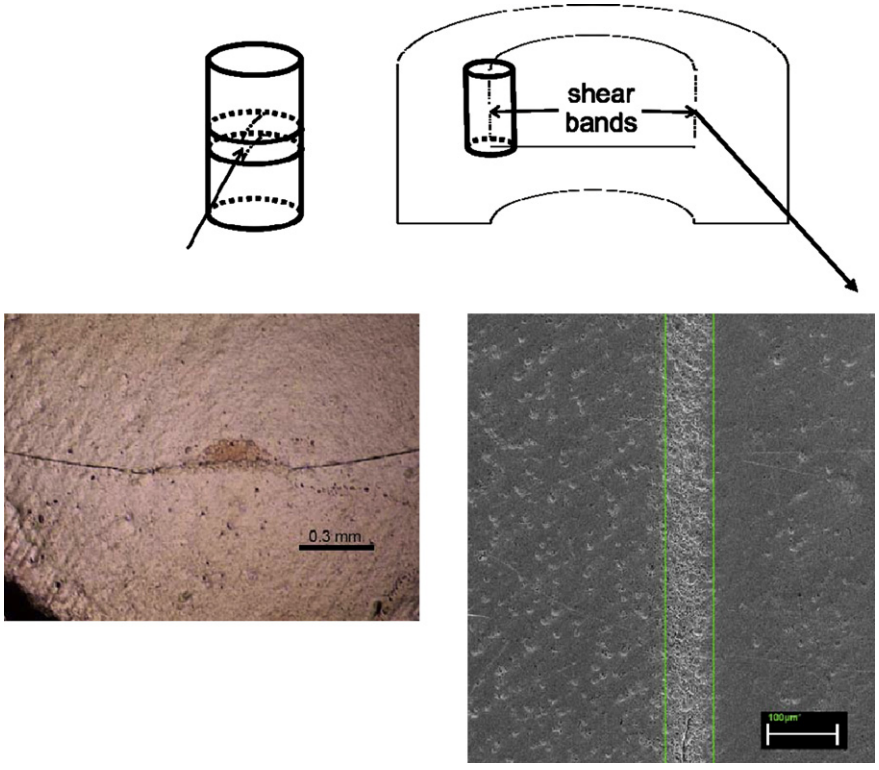

Fig. 8. Optical micrograph of shear bands in deformed hat shaped specimen.

Please cite this article in press as: Mishra A et al., High-strain-rate response of ultra-fine-grained copper, Acta Mater (2008), doi:10.1016/j.actamat.2008.02.023

pressure is now being applied on the compressed flat sample surface and not the hat itself. Two specimens were tested with displacements of 0.5 (3 ring) and 1.5 mm (1 ring). The shear strain in the hat-shaped sample can be estimated by dividing the displacement by the thickness. For the 0.5 mm displacement (3 ring specimen) it is equal to 100.

Fig. 8 shows optical micrographs of the shear band as observed in one of the 3 mm disks that was electropolished to a smooth shiny finish. A circular shear band is expected in a hat sample and curved segments of this band appear in sectioned TEM rods and disks (left side). A perforation in this sample was created in such a way that the band was located in the thin area next to the hole for TEM analysis. The right-hand side shows the longitudinal section. From the micrograph image, the thickness of the shear band was measured to be 50–60 μm. This is in contrast to the values reported by Meyers et al. [27] and Andrade et al. [26] for copper. The thickness varied with grain size and pre-deformation of the specimen. For annealed copper, it was ~ 500 μm, decreasing to ~200 μm for shock-hardened copper. It was also shown by Andrade et al. [26] that the boundary between the plastic shear and undeformed regions in a shock-hardened sample is sharp while a well-annealed sample had a more diffuse plastic deformation region. Fig. 9a and b shows SEM micrographs of about half the shear band width.

In the shear band, the time for heat conduction decreases as the strain rate increases, leading to higher temperatures (at the same strain) at higher strain rates. Bai et al. [47] obtained the following approximate equation for δ, the width of the shear band:

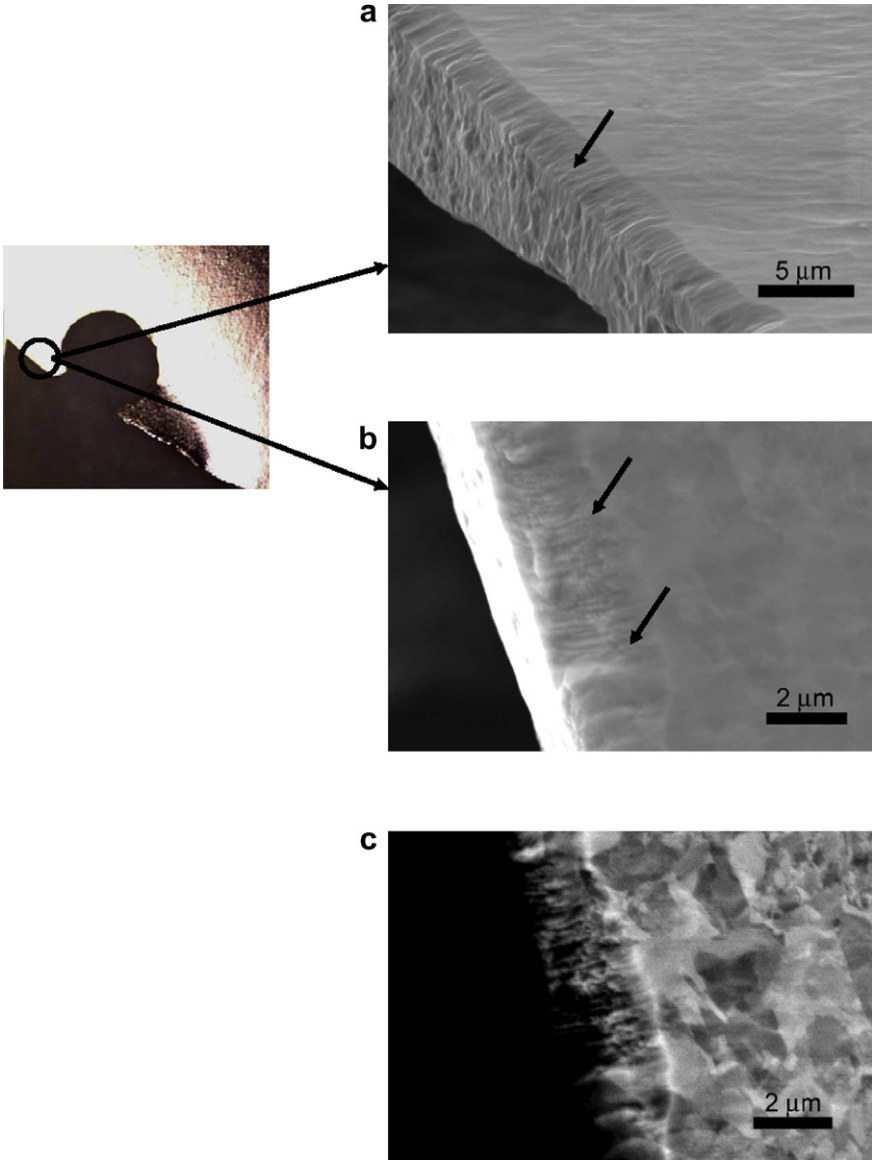

Fig. 9. (a), (b) SEM images of the shear band in a foil that cleaved along the shear band, and (c) recrystallized grain structure visible inside the shear band shown by backscatter image of (b).

Please cite this article in press as: Mishra A et al., High-strain-rate response of ultra-fine-grained copper, Acta Mater (2008), doi:10.1016/j.actamat.2008.02.023

$$\delta \cong 2\left(\frac{\lambda T}{\tau\dot{\gamma}}\right)^{1/2} \quad (4)$$

where λ is the thermal conductivity ($=10.3 \times 10^{-4}$ m^2 s^{-1}) and T, τ and $\dot{\gamma}$ are the temperature, stress, and strain rate inside the shear band.

Grady [48] has another equation, of the form

$$\delta = \left(\frac{9\rho^3 C_p^2 \lambda^3}{\tau^3 \alpha^2 \dot{\gamma}}\right)^{1/4} \quad (5)$$

where α is the thermal softening rate, assuming linear behavior ($\tau = \tau_0(1 - \alpha T)$) and the other parameters were previously defined. Grady [49] later proposed another equation, where the term 9 is replaced by 16.

Fig. 10 shows the prediction from the above equations and the as-measured shear band thickness from experiments. Wright [50] states that the agreement of the Bai equation with experimental results is usually within a factor of 2. For the experiments carried out by Andrade et al. [26], there is a reasonable correspondence with both Bai's [47] and Grady's [48] equations . The trend of the experimental data parallels the two equations. Although both Bai's and Grady's equations predict a decrease in band thickness with increasing flow stress, the precipitous drop for the UFG copper has to be attributed to an additional mechanism for the loss of mechanical stability. This can be due to the increased propensity of thermal softening in ECAP samples. In the original formulation of Grady [48] this parameter assumes a linear thermal softening with the melting point marking the zero strength value; this provides a value of $\alpha = 8.8 \times 10^{-4}$ K^{-1}. The results are given in Eq. (1) in Fig. 10. In order to simulate a more drastic thermal softening of the UFG copper, consistent with the microstructural instability, it is assumed that the full softening is achieved at 400 K. This corresponds to $\alpha = 2.5 \times 10^{-3}$. The results are plotted as Eq. (2) in Fig. 10. Thus, the agreement with the Grady equation for the UFG specimen can be significantly improved by modifying the linear softening parameter α. Wei et al. [8] measured the shear-band widths in iron processed by ECAP to a grain size of 100 nm and found a value of 15 μm which they compared favorably with the Bai equation. However, they used a strain rate higher by three orders of magnitude. The present results, which cover the grain size range from polycrystalline to UFG, definitely point to a change in mechanism.

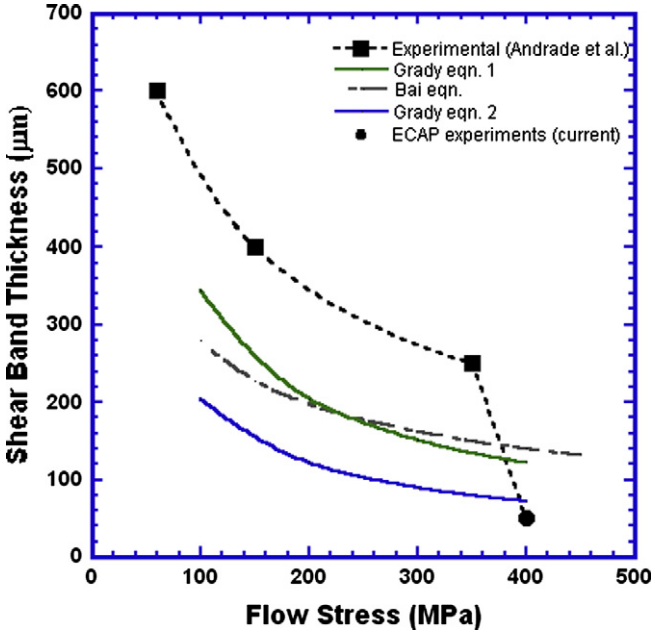

Fig. 10. Shear band thickness obtained from experiments as compared to prediction by Bai's [43] and Grady's [44] equations.

Fig. 11 illustrates the EBSD maps corresponding to the normal direction (ND), transverse direction (TD), and shear direction (SD) in an area spanning the shear band and nearby region. The scan area is shown in Fig. 11d with the shear band to the left end. From the EBSD pattern, large recrystallized grains can be seen in the shear band and the heat-affected zone close to the band. However, most of the grains in the region outside shear band are ultra-fine sized and elongated as is typical of the ECAP microstructure. There is a large scatter in grain sizes ranging from 0.2 μm to 4 μm, where most of the small grain size is retained from ECAP processing and the large grains arise from heat-induced recrystallization within the shear band and heat-affected zone close to the band. This is corroborated by TEM micrographs (Fig. 12a and b) taken from the shear band area and (SEM image in Fig. 9c).

A temperature rise to above 500 K is predicted in the shear band, and this can have a significant effect on its neighboring regions. The observed effect is illustrated in Fig. 13a and b. Recrystallized areas can be seen advancing into the UFG region in Fig. 13a. This is characteristic of migration recrystallization. The size of these recrystallized regions (with diameters of 1–5 μm) is strongly suggestive of an additional post-deformation process. If the temperature rise is sufficiently high after DRX, grain growth can occur during the post-deformation cooling stage. Similar features were observed by Andrade et al. [26,27] in quasi-static deformation of copper in the temperature range 523–573 K. These recrystallized regions are identical to the ones characterized by Wilbrandt et al. [51] in cold worked copper subjected to annealing treatment.

3.3. Reverse Taylor tests

3.3.1. Description of results

Table 1 is a matrix of the samples examined and the individual respective velocities. Reverse anvil-on-rod Taylor impact experiments were performed on the initial Cu specimen at 88 m s^{-1}, the 2-pass ECAP Cu specimen at 123 m s^{-1}, and the 8-pass ECAP Cu specimen at 125 m s^{-1}. Table 2 lists the yield strengths obtained from quasistatic experiments performed on each sample type, and the final axial and transverse (areal) strains for the samples following the reverse Taylor tests. Since the 2-pass and 8-pass specimens were tested at the same velocity, the

Please cite this article in press as: Mishra A et al., High-strain-rate response of ultra-fine-grained copper, Acta Mater (2008), doi:10.1016/j.actamat.2008.02.023

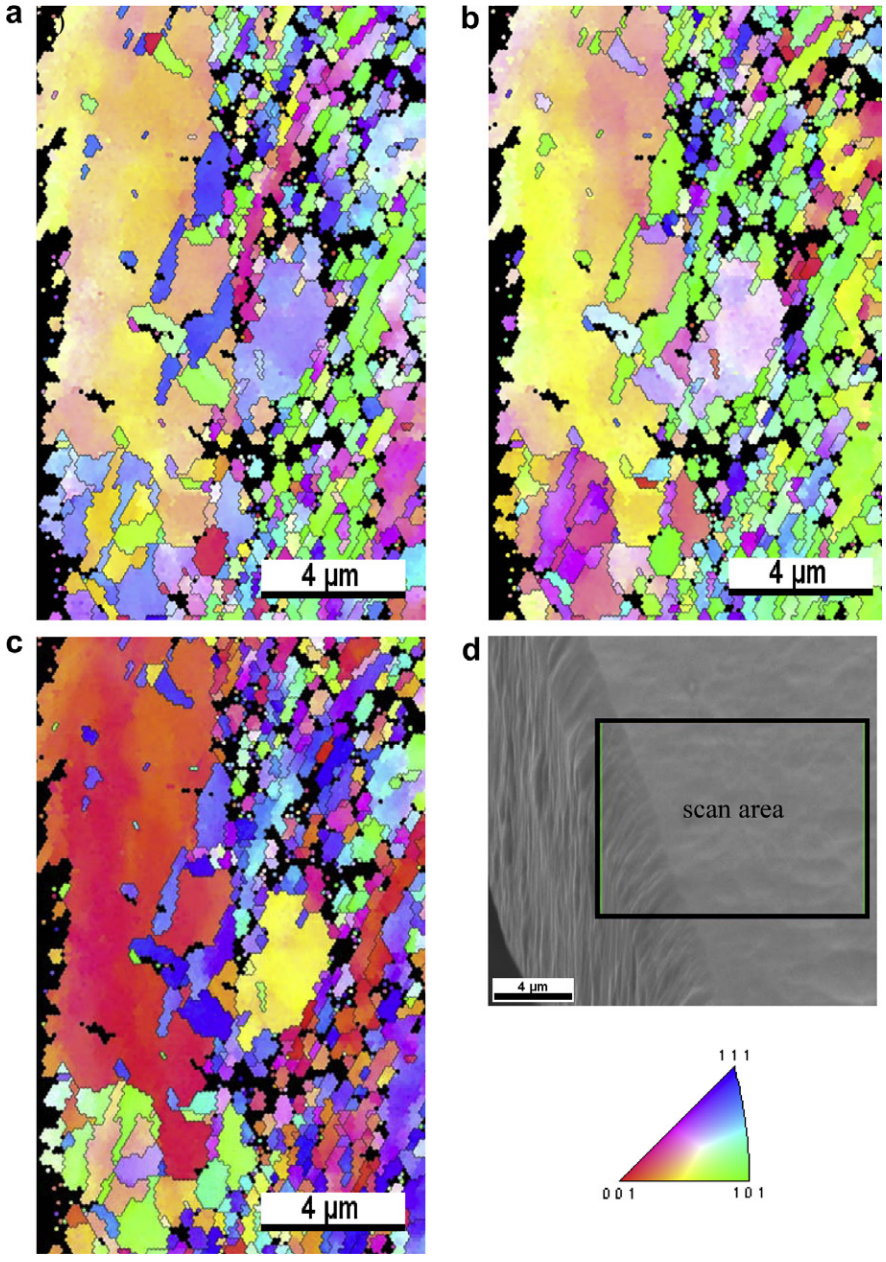

Fig. 11. EBSD maps corresponding to (a) ND, (b) TD, and (c) SD in the area close to the shear band, (d) SEM image showing the EBSD scan area.

amount of strain can be compared, and it is clear that the 8-pass sample is a stronger material, and thus more resistant to deformation.

AUTODYN simulations were performed using the Johnson–Cook constitutive model with hardening constants obtained from stress–strain curves measured at a strain rate of 0.1 s^{-1}, and empirically determined strain rate constants that were modified to fit the free surface velocity traces measured for each experiment. Fig. 14 shows an example of the match between the experimentally measured free surface velocity trace for the three samples, and that obtained from simulation using the Johnson–Cook model. The final values of the Johnson–Cook constants used for comparison of the recorded transient shapes of the specimens with the simulation profiles at corresponding time intervals also show a close correlation with the direct measurements from cylindrical specimens. The fit between experimental (black lines) and calculated (gray lines) free-surface velocities is excellent.

Once the Johnson–Cook equation and constants were validated via correlation with the measured free surface velocity trace and the transient deformation profiles, values of the dynamic yield strength were calculated as listed in Table 2. It can be seen that the 8-pass ECAP sample is consistently stronger than the 2-pass and the as-received Cu samples. The yield strength values are also higher than those obtained at lower strain rates, indicating the effect of strain rate on yield strength (see Table 3).

Please cite this article in press as: Mishra A et al., High-strain-rate response of ultra-fine-grained copper, Acta Mater (2008), doi:10.1016/j.actamat.2008.02.023

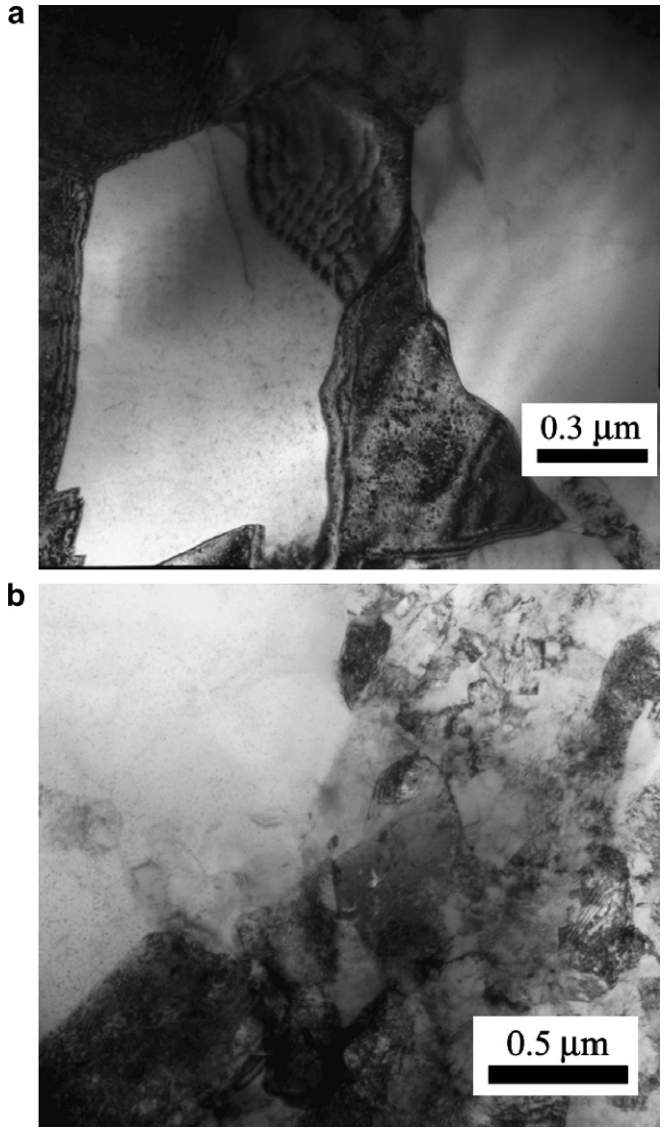

Fig. 12. TEM images of the recrystallized (as a result of severe plastic deformation) microstructure in the shear band of hat-shaped specimens.

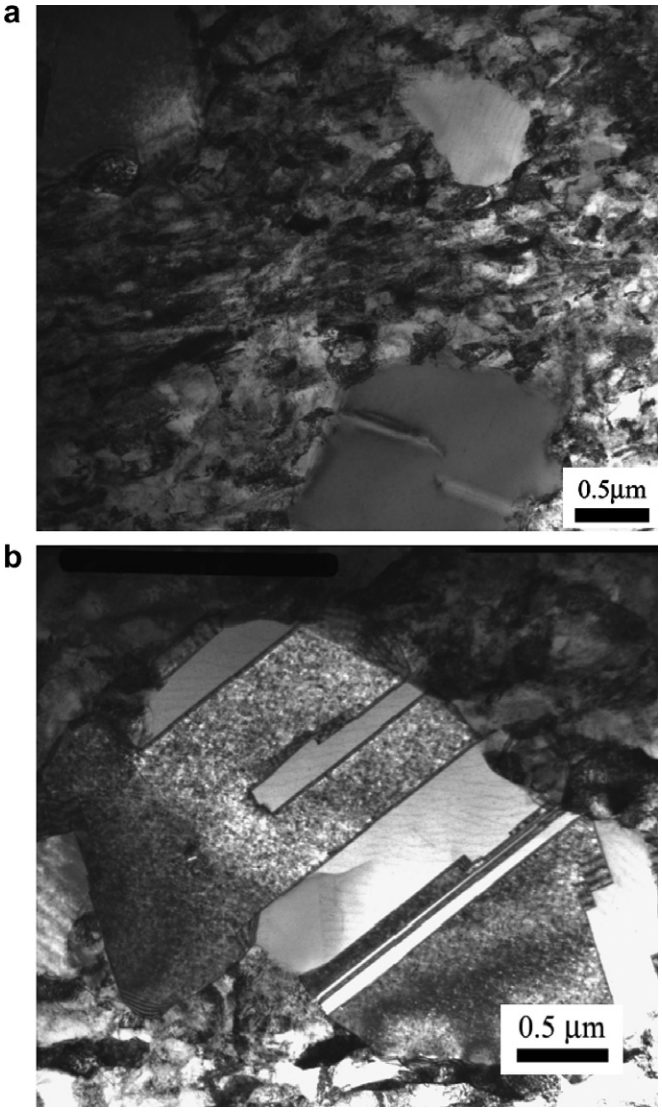

Fig. 13. TEM images of the microstructure close to the shear band.

3.3.2. Transmission electron microscopy

The initial grain size of the copper rod was 30 μm. It was annealed at 500 °C for 1 h under vacuum condition before samples were cut for ECAP. Even after annealing, the initial microstructure had a high dislocation density. Three different conditions (initial, 8 and 16 ECAP passes) were reverse Taylor impacted at the same velocity of 180 m s^{-1} to maximize the microstructural changes. TEM samples were cut in two orthogonal directions from the frontal impact surface of the recovered samples. Cylinders of 3 mm diameter were cut in the transverse (Fig. 15a) and longitudinal (Fig. 15b) directions using electric discharge machining. Fig. 15c shows the region closest to the impact surface along the longitudinal section as imaged by EBSD. The light regions represent individual grains. It can be seen that significant recrystallization occurred with the size of the grains increasing with decreasing distance from the impact interface.

Table 1
Matrix of Taylor samples examined and their individual impact velocities

Impact velocity (m s^{-1})	Initial	2 Passes	8 Passes	16 Passes
88	×			
123		×		
125			×	
180	×		×	×

The microstructure of the initial copper after impact was heavily dislocated. Dislocation cells that existed in the initial structure are now replaced by elongated dislocation laths (Fig. 16). Clearly the dislocation density is much higher than the initial sample and this is a result of the deformation introduced in the sample during impact.

Fig. 17a shows a region of the Taylor impact 8-pass ECAP sample where the grains are ultra-fine sized. This is typical of the microstructure produced at the end of 8 passes. There is a small recrystallized region, marked R. In other places, larger dislocation-free grains were often

Please cite this article in press as: Mishra A et al., High-strain-rate response of ultra-fine-grained copper, Acta Mater (2008), doi:10.1016/j.actamat.2008.02.023

Table 2
Yield stresses from quasistatic and dynamic tests, and reverse Taylor test experiment details for initial, 2- and 8-pass ECAP Cu samples

No. ECAP passes	Quasistatic yield stress ($\dot{\varepsilon} = 4.7 \times 10^{-3}s^{-1}$) (MPa)	Quasistatic yield stress ($\dot{\varepsilon} = 0.1s^{-1}$) (MPa)	Impact velocity ($m\,s^{-1}$)	Axial strain, $\varepsilon = \ln(L_f/L_0)$	Areal strain, $\varepsilon = 1 - A_0/A$	Dynamic flow stress, Johnson–Cook (Eq. 1) ($\dot{\varepsilon} = 1.3 - 1.7 \times 10^{3}s^{-1}$) (MPa)
0	298	319	88	0.137	0.377	427
2	371	392	123	0.177	0.549	513
8	397	430	125	0.169	0.518	571

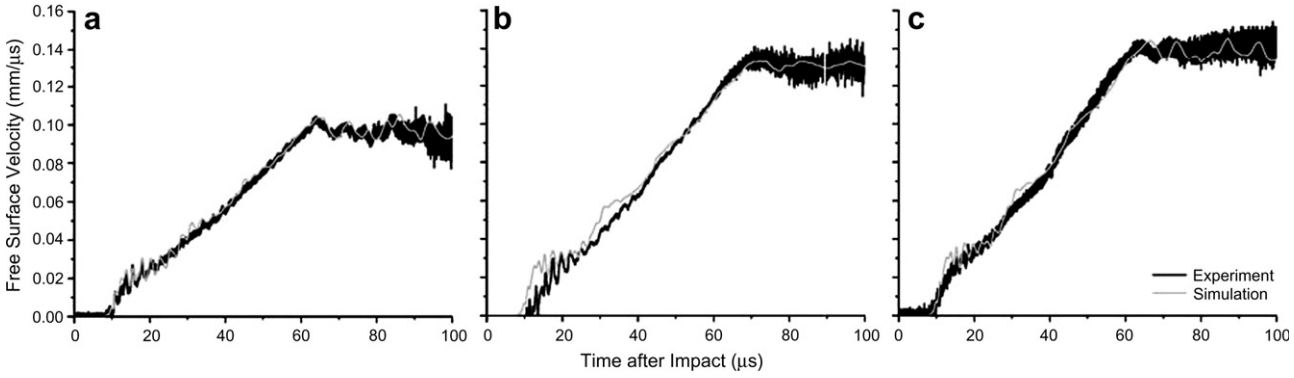

Fig. 14. Simulated vs. experimental free surface velocity trace for Cu specimens. Simulation is based on modified Johnson–Cook parameters from stress–strain data and empirical fit to the experimental free surface velocity trace. (a) Initial Cu, 88 m/s, (b) 2- pass Cu, 123 m/s, and (c) 8-pass Cu, 125 m/s.

Table 3
Table of modified J–C parameters

No. ECAP passes	Yield stress, A (MPa)	Hardening constant, B (MPa)	Hardening exponent, n	Strain rate constant, C	Thermal softening exponent, m
0	90	340	0.0334	0.009	1.09
2	90	390	0	0.011	1.09
8	90	423	0	0.017	1.09

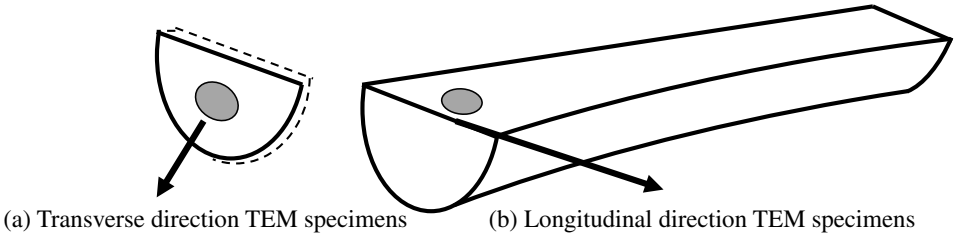

(a) Transverse direction TEM specimens (b) Longitudinal direction TEM specimens

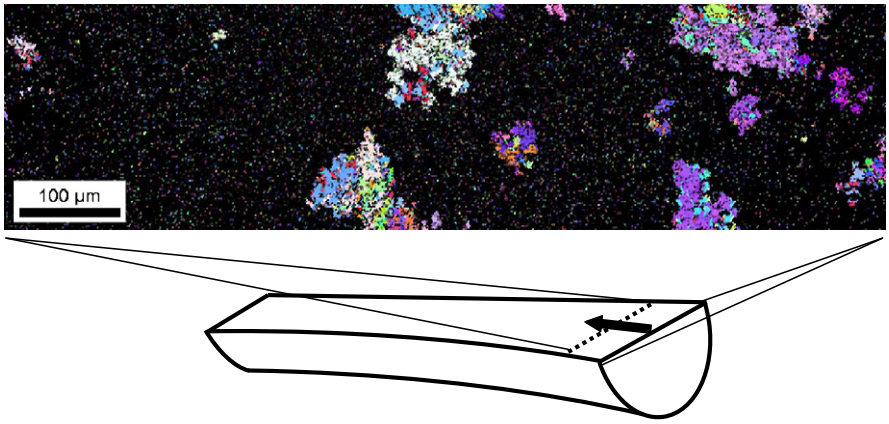

(c)

Fig. 15. (a and b), Orientations of TEM samples cut from cylindrical specimen after reverse Taylor impact; (c) change in microstructure as a function of distance from impact surface; light regions represent new grains.

Please cite this article in press as: Mishra A et al., High-strain-rate response of ultra-fine-grained copper, Acta Mater (2008), doi:10.1016/j.actamat.2008.02.023

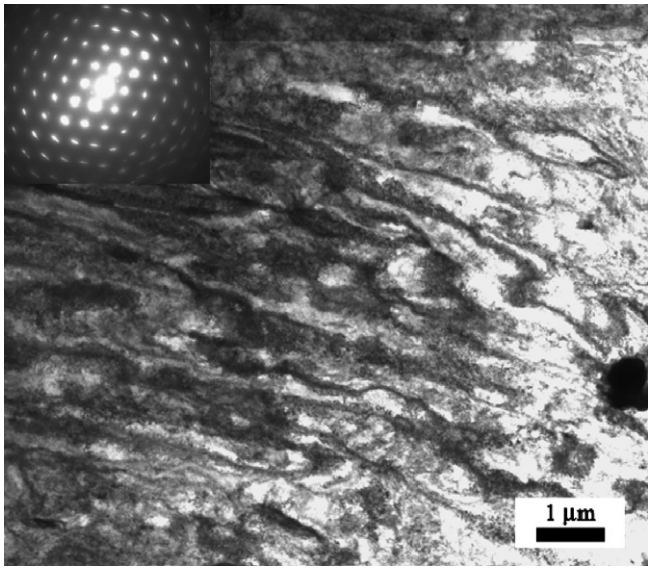

Fig. 16. Microstructure of the Taylor impact specimen.

observed adjacent to a heavily dislocated UFG region as shown in Fig. 17 (b–d). These are recrystallized grains that were formed during or immediately after Taylor impact triggered by the temperature rise during impact. Fig. 17b is a low magnification image of large recrystallized grains in a region of heavily deformed ultra-fine grains. From these micrographs, it can be concluded that a possible growth pattern of recrystallized grains is one in which these new grains sweep through the ultra-fine region thus replacing it by large, dislocation-free grains. Fig. 17c shows a large recrystallized grain surrounded by a matrix of UFG microstructure. The size of these recrystallized grains varies depending on when the nucleation of these new grains took place in the Taylor impact process. The features within these recrystallized grains show twins and stacking faults (e. g. Fig. 17d), typical of recrystallization features in fcc metals [48].

Fig. 18a shows the typical UFG microstructure in the 8-pass ECAP sample (transverse section). The corresponding selected area diffraction pattern (SADP) shows a ring-like

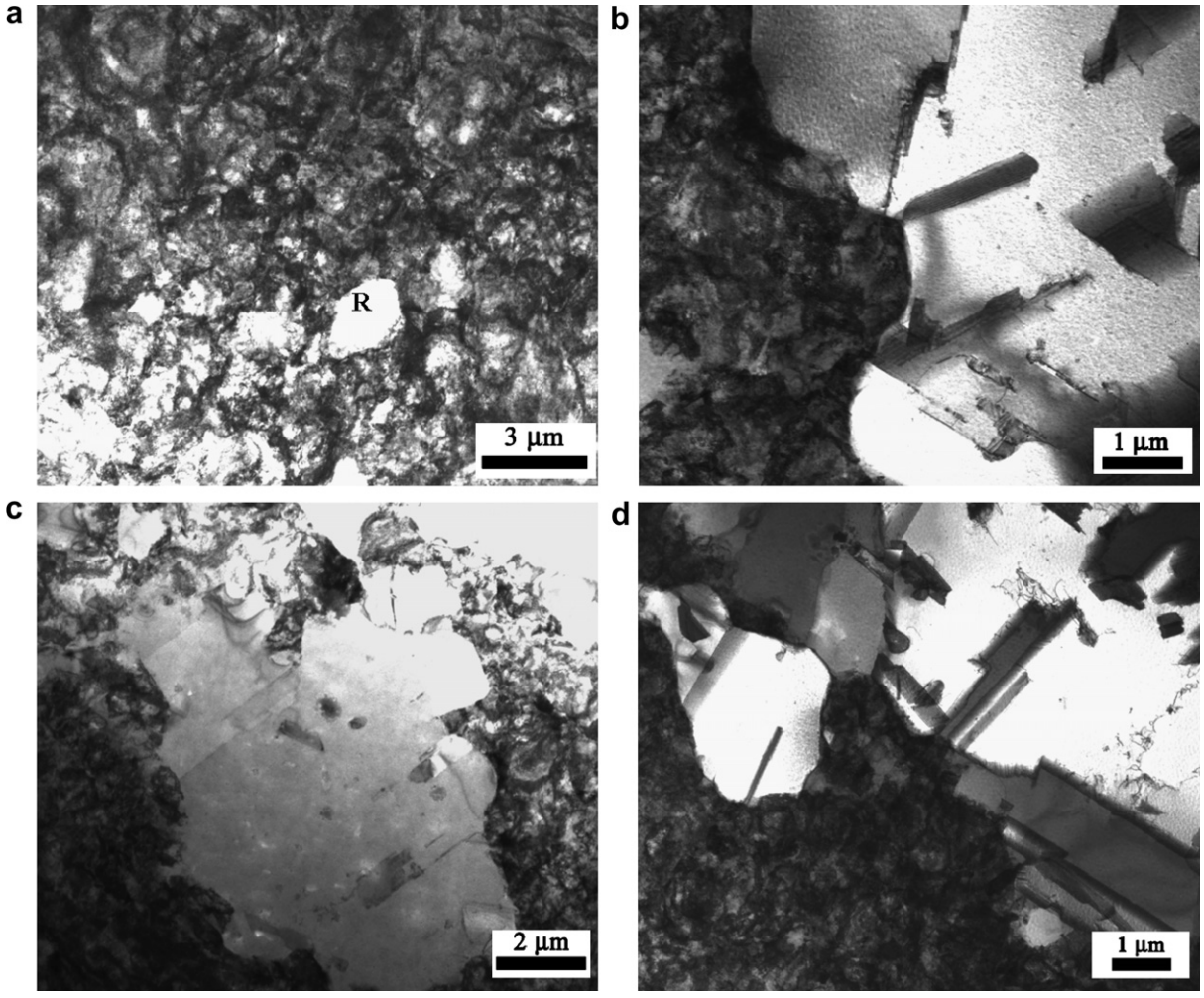

Fig. 17. Longitudinal section (in Taylor impact specimen); (a) deformed region showing one apparently recrystallized grain (marked by R); (b–d) recrystallized grains in heavily deformed ultra-fine grain microstructure (8 passes); and (d) annealing twins in the large recrystallized grains.

Please cite this article in press as: Mishra A et al., High-strain-rate response of ultra-fine-grained copper, Acta Mater (2008), doi:10.1016/j.actamat.2008.02.023

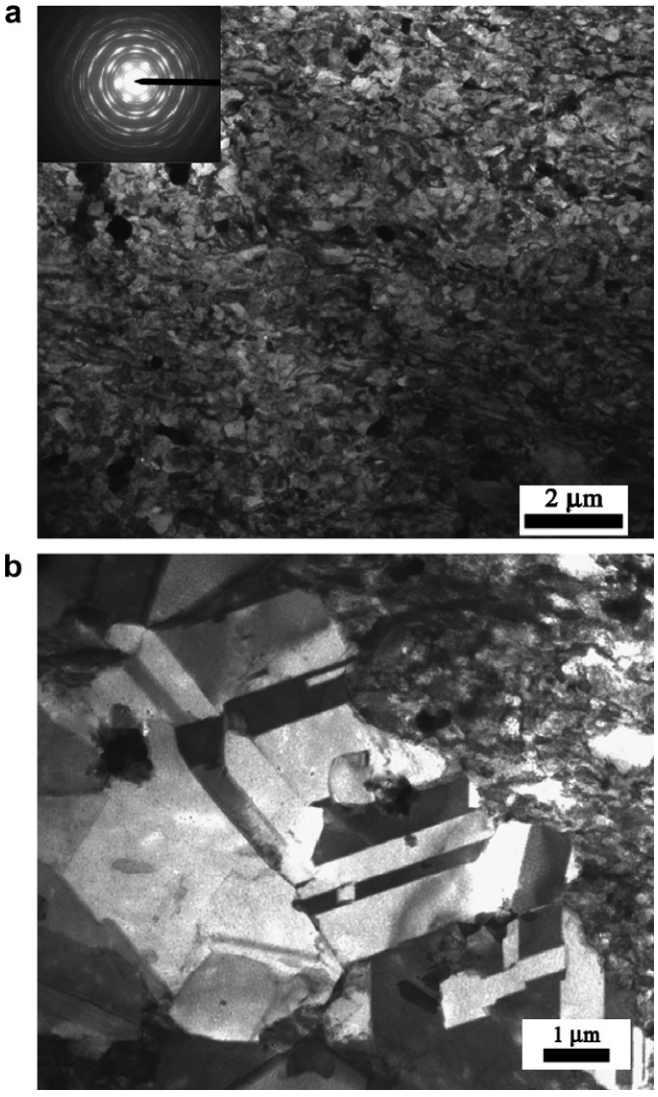

Fig. 18. Transverse section (in Taylor impact specimen); (a) Ultra-fine grained microstructure typical of ECAP; and (b) recrystallized grains with annealing twins in the transverse section of the Taylor shot ECAP sample.

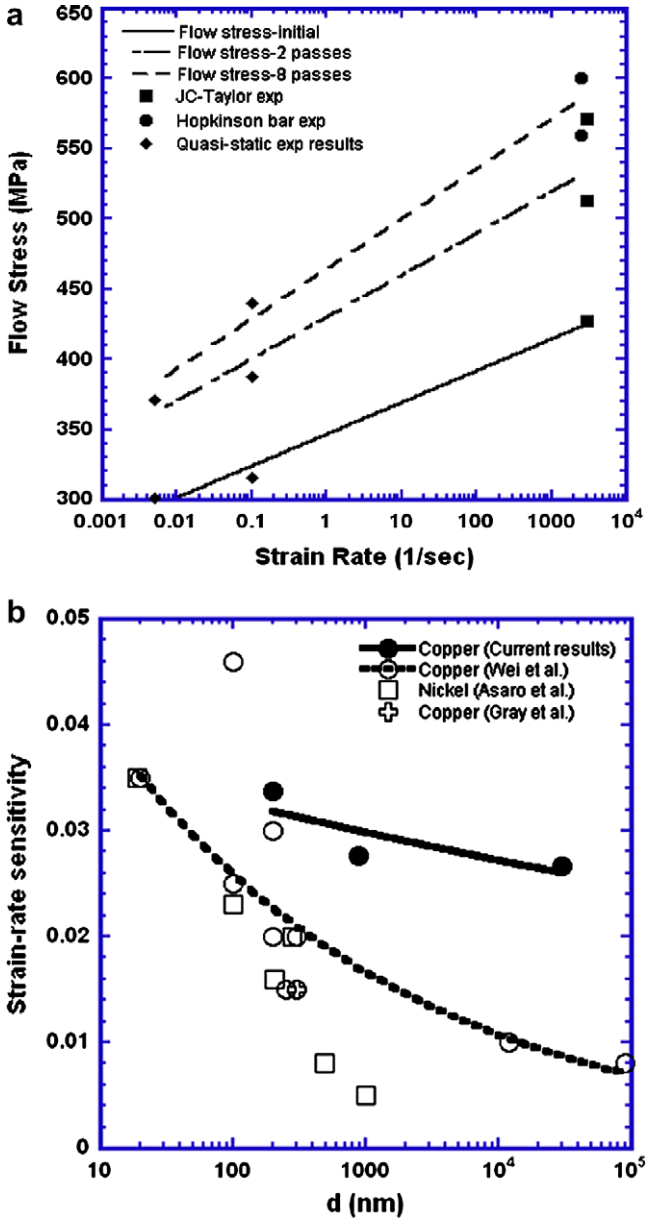

Fig. 19. (a) Strain-rate dependence of flow stress of copper; and (b) strain-rate sensitivity, $\partial \ln \sigma / \partial \ln \dot{\varepsilon}$, as a function of grain size.

pattern indicating that the microstructure consists of ultra-fine grain sizes. Other regions of this transverse section sample, however, show similar extent of recrystallization as seen in the longitudinal section. Fig. 18b shows several fully developed annealing twins in the recrystallized grains.

3.4. Strain-rate sensitivity

The combined results from Hopkinson bar tests on cylindrical specimens and Johnson–Cook predictions from the reverse Taylor experiments are shown in Fig. 19a. The results are consistent although the J–C predictions fall slightly below the dynamic flow stress directly measured from the Hopkinson bar experiments. A linear fit is drawn in Fig. 19a between the two results. The slopes of these lines provide the strain-rate sensitivity. There is a slight but clear increase in strain-rate sensitivity for the 8-pass sample, in comparison with the initial condition. The strain-rate sensitivity is plotted in Fig. 19b and compared with the literature, in particular Wei et al. [8] and Gray et al. [6]. The current values of the strain-rate sensitivity are higher than the reports by Wei et al. [8] and May et al. [9]. However, the trend is consistent: an increased strain-rate sensitivity in the UFG and nanocrystalline region. For comparison purposes data on nickel by Asaro and Suresh [7] are also given. They follow the same pattern.

4. Conclusions

The purpose of the present work was to investigate the response of UFG copper at high-strain-rates. ECAP copper specimens were subjected to three different types of testing: Hopkinson bar compression testing of cylindrical

Please cite this article in press as: Mishra A et al., High-strain-rate response of ultra-fine-grained copper, Acta Mater (2008), doi:10.1016/j.actamat.2008.02.023

samples, Hopkinson bar compression testing of hat-shaped samples and reverse Taylor testing of ECAP specimens. The conclusions are as follows:

1. There is a significant jump in the strength of UFG copper in going from quasistatic to dynamic strain rate tests which is indicative of high-strain-rate sensitivity. This is validated by reverse Taylor test results. Strain-rate sensitivities of ECAP copper after 0, 2 and 8 passes are reported to be 0.027, 0.028 and 0.034.
2. The modified Johnson–Cook equation provides a good fit to the response of the reverse Taylor test impacted copper.
3. Recovered specimens from Taylor and dynamic cylindrical tests exhibit clear evidence of recrystallization at the impact surface. The recrystallized structure is characterized by large grains with a profusion of annealing twins and is thought to develop during and after deformation by dynamic recrystallization. The calculated temperature rise in the cylindrical specimens was ~60 K and, therefore, the structure is considerably more unstable than that of conventional polycrystalline copper, which requires ~100 K for static recrystallization.
4. Shear bands with thickness of ~60 μm were formed in hat-shaped ECAP specimen. The microstructure in the shear band and neighboring areas shows heavy recrystallization due to temperature rise during impact. The morphology of these recrystallized regions is analogous to that in the cylindrical and Taylor specimens.
5. The thickness of the forced band in the UFG copper is much smaller than the predictions from the Bai and Grady equations, which are in reasonable agreement with the shear bands for conventional polycrystalline copper. It is proposed that the accelerated thermal softening of UFG copper plays a significant role in decreasing the shear band thickness. This decrease in shear band thickness is also observed for bulk metallic glasses and was analyzed by Dai et al. [52] and Liu et al. [53], who attributed it partially to an accelerated softening.

Acknowledgements

This UCSD portion of this work was supported by the Office of Naval Research MURI Award N00014-07–1-0740 and National Science Foundation under Grant CMS-0210173 (NIRT). The GIT component was funded by ARO Grant No. E-48148-MS-000-05123-1. We thank Profs. R.J. Asaro, V.F. Nesterenko, and T.G. Langdon for helping us with the ECAP unit and Prof. M.E. Kassner for fruitful discussions. The help of Mr. Hussam Jarmakani was especially valuable. Mr. F. Grignon was instrumental in the development of the ECAP setup. We gratefully acknowledge Prof. K. Vecchio and Dr. Jiang for carrying out part of the high-strain-rate tests. Electron microscopy was conducted at the SHaRE User Facility, which is sponsored at Oak Ridge National Laboratory by the Division of Scientific User Facilities, US Department of Energy.

References

[1] Gleiter H. Prog Mater Sci 1989;33:223–315.
[2] Weertman J. In: Koch, editor. Nanostructured materials. Norwich, NY: Noyes; 2002. p. 393–417.
[3] Meyers MA, Mishra A, Benson DJ. Prog Mater Sci 2006;51:427–556.
[4] Meyers MA, Mishra A, Benson DJ. JOM 2006(April):41–8.
[5] Koch CCI, Ovid'ko A, Seal S, Veprek S. Structural nanocrystalline materials. Cambridge: Cambridge University Press; 2007.
[6] Gray GT, Lowe TC, Cady CM, Valiev RZ, Aleksandrov IV. Nanostruct Mater 1997;9:477.
[7] Asaro RJ, Suresh S. Acta Mater 2005;53:3369.
[8] Wei Q, Cheng S, Ramesh KT, Ma E. Mater Sci Eng A 2004;381:71.
[9] May J, Hoppel HW, Goeken M. In: Horita Z, Langdon TG, editors. Proceedings of the 3rd international conference on nanomaterials by severe plastic deformation, Nanospd 3, Japan; 2005.
[10] Wei Q, Kecskes L, Jiao T, Hartwick KT, Ramesh KT, Ma E. Acta Mat 2004;52:1859–69.
[11] Valiev RZ, Islamgaliev RK, Alexandrov IV. Prog Mater Sci 2000;27:103–89.
[12] Furukawa M, Horita Z, Nemoto M, Langdon TG. J Mater Sci 2001;36:2835.
[13] Furukawa M, Iwahashi Y, Horita Z, Nemoto M, Langdon TG. Mater Sci Eng 1998;A257:328.
[14] Langdon TG, Furukawa M, Nemoto M, Horita Z. JOM 2000;52:30.
[15] Iwahashi Y, Horita Z, Nemoto M, Langdon TG. Acta Mater 1998;46:3317;
Iwahashi Y, Horita Z, Nemoto M, Langdon TG. Mater Sci Eng 1997;A229:23.
[16] Komura S, Horita Z, Furukawa M, Nemoto M, Langdon TG. Metall Mater Trans A 2001;32:707.
[17] Pithan C, Hashimoto T, Kawazoe M, Nagahora J, Higashi K. Mater Sci Eng A 2000;280:62.
[18] Yamashita A, Horita Z, Langdon TG. Mater Sci Eng A 2001;300:142.
[19] Valiev R. Nature Mat 2004;3:511–6.
[20] Mishra A, Kad BK, Gregori F, Meyers MA. Acta Mater 2007;55:13.
[21] Meyer LW, Manwaring S. In: Metallurgical applications of shock-wave and high-strain-rate phenomena. New York: Marcel Dekker; 1986. p. 657.
[22] Beatty JH, Meyer LW, Meyers MA, Nemat-Nasser S. In: Metallurgical applications of shock-wave and high-strain-rate phenomena. New York: Marcel Dekker; 1992.
[23] Lins JFC, Sandim HR, Kestenbach H-J, Raabe D, Vecchio KS. Mater Sci Eng A 2007;457:205–11.
[24] Chen Y-J, Meyers MA, Nesterenko VF. Mater Sci Eng 1999;A268:70.
[25] Meyers MA, LaSalvia JC, Nesterenko VF, Chen YJ, Kad BK. In: McNelley TR, editor. Rex '96, Monterey; 1997. p. 27.
[26] Andrade UR, Meyers MA, Vecchio KS, Chokshi AH. Acta Metall Mater 1994;42:3183.
[27] Meyers MA, Andrade U, Chokshi AH. Metall Mater Trans A 1995;26A:2881.
[28] Xu YB, Zhong WL, Chen YJ, Shen LT, Liu Q, Bai YL, et al. Mater Sci Eng 2001;A299:287.
[29] Meyers MA, Perez-Prado MT, Xue Q, Xu Y, McNelley TR. Acta Mater 2003;51:1307.
[30] Xue Q, Cerreta EK, Gray GT. Acta Mat 2007;55:691.
[31] Meyers MA, Subhash G, Kad BK, Prasad L. Mech Mater 1994;17:175.
[32] Kad BK, Gebert J-M, Perez-Prado MT, Kassner ME, Meyers MA. Acta Mater 2006;54:4111–27.
[33] Taylor GI. Proc Royal Soc Lond A 1948;194:289.

[34] Johnson GR, Cook WH. In: Proceedings of the 7th international symposium on ballistics, The Netherlands; 1983.
[35] Eakins D, Thadhani NN. Int J Impact Eng 2007;34:1821.
[36] Martin M, Mishra A, Meyers MA, Thadhani NN. Mater Sci Eng A 2007;464:202.
[37] Lassila DH, Shen T, Cao BY, Meyers MA. Metall Mater Trans 2004;35A:2729.
[38] Molodova X, Gottstein G, Winning M, Hellmig RJ. Mater Sci Eng A 2007;460–461:204.
[39] Hebesberger T, Stüwe HP, Vorhauer A, Wetscher F, Pippan R. Acta Mat 2005;53:393.
[40] Estrin Y, Isaev NV, Lubenets SV, Malykhin SV, Pugachov AT, Pustovalov VV, et al. Acta Mater 2006;54:5581.
[41] Haouaoui M, Hartwig KT, Payzant EA. Acta Mater 2005;53:801.
[42] Skrotzki W, Scheerbaum N, Oertel CG, Massion RA, Suwas S, Toth LS. Acta Mater 2007;55:2211.
[43] Murr LEE, Trillo A, Pappu S, Kennnedy C. J Mater Sci 2002;37:3337.
[44] Murr LE, Esquivel EV. J Mater Sci 2004;39:1153–68. 15.
[45] Esquivel EV, Murr LE. Mater Sci Tech 2006;22:438–52.
[46] Murr LE, Pizana C. Met Mater Trans 2007;38A:2611–28.
[47] Bai Y, Cheng C, Yu S. Acta Mech Sini 1986;2:1.
[48] Grady DE. Mechanics of materials 1994;17:289.
[49] Grady DE. In: TMS symposium on dynamic behavior of materials, Warrendale, PA, TMS; 2007.
[50] Wright TW. The physics and mathematics of adiabatic shear bands. Cambridge: Cambridge University Press; 2002. p. 176, 177.
[51] Wilbrandt PJ, Haasen P. Z Metall 1980;71:385.
[52] Dai LH, Yan M, Liu LF, Bai YL. Appl Phys Lett 2005;87:14196.
[53] Liu LF, Dai LH, Bai YL, Wei BC. J Non-Cryst Sol 2005;351: 3259.

Please cite this article in press as: Mishra A et al., High-strain-rate response of ultra-fine-grained copper, Acta Mater (2008), doi:10.1016/j.actamat.2008.02.023